Article

OculusGraphy: Signal Analysis of the Electroretinogram in a Rabbit Model of Endophthalmitis Using Discrete and Continuous Wavelet Transforms

Aleksei Zhdanov [1,2,*], Paul A. Constable [3], Sultan Mohammad Manjur [4], Anton Dolganov [2], Hugo F. Posada-Quintero [4], Aleksander Lizunov [5]

[1] Machine Learning and Data Analytics Lab, University of Erlangen-Nuremberg, 91052 Erlangen, Germany
[2] Engineering School of Information Technologies, Telecommunications and Control Systems, Ural Federal University Named after the First President of Russia B. N. Yeltsin, 620002 Yekaterinburg, Russia
[3] College of Nursing and Health Sciences, Caring Futures Institute, Flinders University, Adelaide, South Australia, Australia
[4] Department of Biomedical Engineering, University of Connecticut, Storrs, CT 06269, USA
[5] Department of Functional Diagnostics, IRTC Eye Microsurgery Ekaterinburg Center, 620149 Yekaterinburg, Russia
* Correspondence: aleksei.e.zhdanov@fau.de

Abstract: Background: The electroretinogram is a clinical test used to assess the function of the photoreceptors and retinal circuits of various cells in the eye, with the recorded waveform being the result of the summated response of neural generators across the retina. Methods: The present investigation involved an analysis of the electroretinogram waveform in both the time and time-frequency domain through the utilization of the discrete wavelet transform and continuous wavelet transform techniques. The primary aim of this study was to monitor and evaluate the effects of treatment in a New Zealand rabbit model of endophthalmitis via electroretinogram waveform analysis and to compare these with normal human electroretinograms Results: The wavelet scalograms were analyzed using various mother wavelets, including the Daubechies, Ricker, Wavelet Biorthogonal 3.1 (bior3.1), Morlet, Haar, and Gaussian wavelets. Distinctive variances were identified in the wavelet scalograms between rabbit and human electroretinograms. The wavelet scalograms in the rabbit model of endophthalmitis showed recovery with treatment in parallel with the time -domain features. Conclusions: The study compared Adult, Child, and Rabbit electroretinogram responses using DWT and CWT, finding that Adult signals had higher power than Child signals, and Rabbit signals showed differences in a-wave and b-wave depending on the type of response tested, while Haar Wavelet was found to be superior in visualizing frequency components in electrophysiological signals in following the treatment of endophthalmitis and may give additional outcome measures for the management of retinal disease.

Keywords: biomedical research; electroretinography; electroretinogram; ERG; electrophysiology

1. Introduction

1.1. Electroretinogram

The electroretinogram (ERG) is a functional test of the retina that is used clinically [1] to assesses principally the function of the photoreceptors and the retinal circuits of horizontal, bipolar, Müller, amacrine and ganglion cells. The relative contribution of each cell depends upon the state of retinal adaptation, flash color, strength, duration, and stimulus frequency [2]. In the standard full-field ERG the recorded waveform is the result of the summated response of the neural generators across the entire retina. Granit first elucidated that the ERG waveform was the sum of parts through analysis of the dark adapted (DA) ERG in a series of animal studies using increasing degrees of anesthesia [3]. The ERG waveform typically consists of an initial negative trough termed the 'a-wave' which is followed by

a positive peak known as the 'b-wave'. The a-wave represents hyperpolarization of the photoreceptors (rods or cones depending on the degree of retinal adaptation) [4] - [6]. The 'b-wave' has many neural contributors, including the depolarization of the bipolar cells [7,8] Muller cell glial potassium currents [9] and inhibitory horizontal cells [10,11] that all contribute to the main b-wave peak amplitude and timing. In addition, under light adapted (LA) conditions the a-wave also receives contribution from post-receptoral neurons that influence the amplitude [12] - [14]. Inhibitory horizontal cells also provide feedback inhibition to photoreceptors under LA and DA conditions [15,16]. The descending limb of the b-wave is mainly shaped by ganglion cells and forms the photopic negative response [17] that is not considered in this analysis. Finally, on the ascending limb of the b-wave 2-3 small peaks are observed which are known as the oscillatory potentials (OPs) that originate in amacrine cells with contributions from bipolar and ganglion cells that contribute to the high frequency components of the ERG waveform and are typically analyzed after band-pass filtering the raw ERG signal [18] - [22]. The rabbit ERG has been used extensively in studies of drug toxicity and diseases of the retina and has a similar shape to the human ERG [23] - [27].

1.2. Analysis of the electroretinogram waveform

To develop the clinical applicability of the ERG, several strategies have been employed to analyze features of the waveform and their response to different flash strengths. For example the a-wave's kinetics has been mathematically modelled [28] - [30] and the OPs have been analyzed using the integrated root-mean-square of their amplitudes [1] and wavelet analyses [31,32]. The modelling of the ERG b-wave amplitudes as the photopic hill under LA [33,34] and as a more complex luminance response function under DA [35] conditions has also been used in clinical studies [36] - [38].

The application of signal analysis to the ERG waveform was developed by Gauvin who applied a discrete wavelet transform (DWT) analysis to extract energies corresponding to the ON- and OFF- pathways of the a- and b-waves as well as the early and later OPs [39] - [41]. The DWT application of Gauvin's work has been applied to the identification of neurodevelopmental and retinal disease [42] - [45] and offers the potential to develop the scope of practice for the ERG [46].

In this study we analyzed the ERG waveform in the time and time frequency domain using DWT and Continuous wavelet transforms (CWT) to monitor the effects of treatment in an experimental rabbit model of endophthalmitis. The application of signal analysis may provide additional and complimentary information about the underlying neural generators of the ERG and supports the advancement of the use of the ERG as a clinical test of retinal and central nervous system function [55,56].

2. Materials and Methods

2.1. Study protocol and signals

All recordings were made with the Tomey GmBH EP-1000 stimulator sampling at 2 kHz with 0.1-300 Hz bandpass filter. The two flash strengths were the DA 2.0 ERG (Scotopic Response) and light adapted (LA) 2.0 ERG (Maximal Response) stimuli were a white 2 cd.s.m-2 on a 0 cd.m-2 background. Loop electrodes positioned in the lower lid were used for human recordings and ERG-Jet lens electrodes were used for rabbit recordings that have an excellent an signal-to-noise ratio [47]. Oxybuprocaine 0.4% was used to dilate the pupils in human and rabbit subjects. The use of oxybuprocaine 0.4% for pupil dilation has been well-documented in human and animal studies, and its safety and efficacy have been established. In addition, the short duration of action of oxybuprocaine makes it a preferred choice for ophthalmic procedures where rapid onset and quick recovery of normal function are desired. The experimental protocols are described in Table 1 with all signals amplified and digitized using the EP-1000 system's built-in amplifier and A/D converter [48].

To compare human ERG signals and use the signals of the Scotopic Response protocol shown in Figure 1a and Maximum Response protocol shown in Figure 1b. Figure 1 shows

Table 1. Characteristics of an electrophysiological study.

	Scotopic 2.0 ERG Response	Maximum 2.0 ERG Response
Flash intensity, cd·s·m-2	2	2
Background light, cd·s·m-2	0	0
Flash duration, ms	0.5	3
Flash frequency, kHz	20	20
Stimulus interval, s (cps)	2.5 (0.4)	10 or 13 (0.1)
Flash color	white	white

the signals of healthy objects. Table 2 provides information on the age of objects, as well as the values of the following parameters: *a* - amplitude of the a-wave, *b* - amplitude of the b-wave, *la* - latency of the a-wave, *lb* - latency of the b-wave.

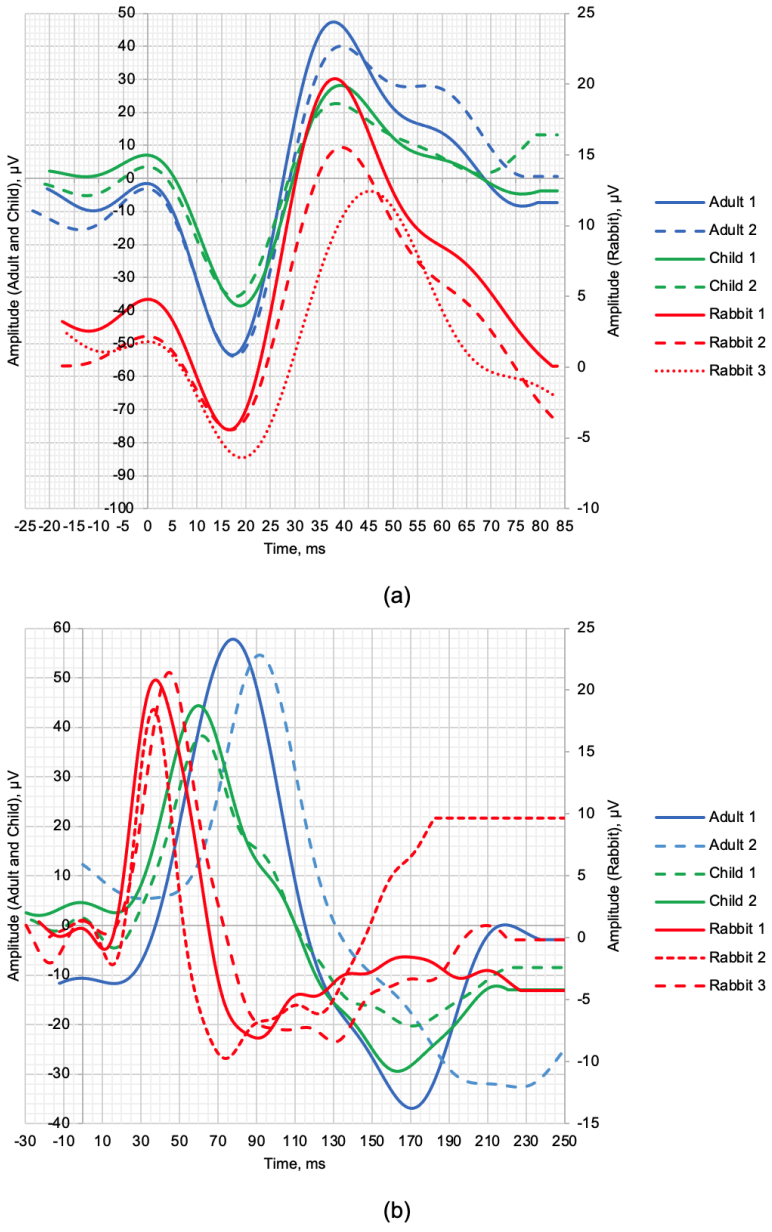

Figure 1. ERG signals time-domain representation of healthy objects: (**a**) Scotopic 2.0 ERG Response. (**b**) Maximum 2.0 ERG Response.

Table 2. Scotopic 2.0 ERG Response and Maximum 2.0 ERG Response parameters of healthy objects.

	Adult 1	Adult 2	Child 1	Child 2	Rabbit 1	Rabbit 2	Rabbit 3
Age	20.5 y.o.	27.8 y.o.	10.9 y.o.	7.5 y.o.		2-3.5 mos.	
				Maximum 2.0 ERG Response			
a, µV	52.32	50.69	45.65	39.28	9.18	6.59	8.2
b, µV	101.22	93.78	66.74	58.35	24.75	19.92	18.86
la, ms	17.5	18	19	18	16.5	17	19.5
lb, ms	38	39.5	39.5	38.5	38	39.5	45.5
				Scotopic 2.0 ERG Response			
a, µV	1.04	-	6.05	2.03	1.82	3.47	1.04
b, µV	69.53	60.01	42.77	46.91	21.87	20.47	21.12
la, ms	17	-	16	16.5	10.5	14.5	12.5
lb, ms	78	92.5	62.5	60.5	38.5	37.5	44.5

The average values of the Scotopic 2.0 ERG Responses are presented in Table 2 showed the amplitude of the a-wave of adults (children) was 5.4 (4.3) times higher than the amplitude of the a-wave of rabbits, the b-wave is 3.6 (1.9) times slower. The time to peaks of the a- and b-waves differed by no more than 5.4%. The average Maximum 2.0 ERG Response parameters are shown in Table 2 shows that the amplitude of the b-wave of adults (children) was 67.34% (52.82%) higher than the amplitude of the b-wave of rabbits. Analysis of the a-wave was not performed due to the weak response of the photoreceptors at this flash strength. The average values of the time to peak of the b-wave of adults (children) relative to the time to peak of the b-wave of the rabbits differed by 52.88% (34.68%) delayed.

To further explore the time-frequency domain analysis of the ERG waveforms, we used DWT and CWT analysis using the following mother wavelets:

1. Daubechies Wavelet
2. Ricker Wavelet
3. Wavelet Biorthogonal 3.1 (bior3.1)
4. Morlet Wavelet
5. Haar Wavelet
6. Gaussian Wavelet

The above mother wavelets were used for the processing and analysis of ERGs in previous studies since 2000 [49]. Therefore, it was necessary to determine the optimal mother wavelet for the Maximum 2.0 ERG Response and Scotopic 2.0 ERG Response used in this study.

2.2. Endophthalmitis treatment in rabbit

12 New Zealand rabbits (male), weighing from 3.0 to 3.2 kg (average 3.10 ± 0.35 kg), aged 2 to 3.5 months had treatment for bacterial endophthalmitis of the right eye associated with staphylococcus aureus. Each rabbit was injected with a solution of quantum dots 0.01% dose of QD InP/ZnSe/ZnS 660 in combination with Vancomycin 10 mg/ml [50]. Article [59] provides an exploration of the evaluation of ophthalmotoxicity stemming from quantum dots based bioconjugates, pertaining to their potential in the treatment of resistant endophthalmitis. This research was conducted using rabbits, with the inclusion of normal rabbit ERG controls. In all cases, the volume of substance for intraocular administration was 0.1 ml (0.05 + 0.05 ml.). The solution was injected intravitreally into the right eye of the animal. During the study, slit-lamp photography (SLP) of the anterior segment, optical coherence tomography (OCT) of the posterior segment, and ERG recordings were recorded. SLP was produced using a Haag-Streit slit lamp BQ 900 manufactured by Haag-Streit Holding AG. OCT was performed using an Optovue RTVue-100 manufactured by Optovue Inc. The research involving laboratory animals was conducted in strict adherence to the

principles outlined in the code of ethics, specifically the "Directive 2010/63/EU of the European Parliament and the Council of the European Union".

OCT, SLP and ERG measurements and recordings were performed weekly. The Maximum 2.0 ERG Response and Scotopic 2.0 ERG Response recordings are shown in Figures 2a and Figure 2b. Figure 2 during the treatment period with improvement in the amplitudes of the a- and b-waves. Table 3 provides the values of the following parameters: *a* - amplitude of the a-wave, *b* - amplitude of the b-wave, *la* - latency of the a-wave, *lb* - latency of the b-wave.

The Scotopic 2.0 ERG Response results presented in Table 3 demonstrate the therapeutic effect of the treatment. The values *a*, *b*, *la*, and *lb* registered on 3rd week differ from the average values of healthy rabbits by 26.09%, 12.28%, 11.67%, and 4.88%. Maximum 2.0 ERG Response results are presented in Table 3 also demonstrate the therapeutic effect of the treatment. The values *b* and *lb* registered on 3rd week differ from the average values of healthy rabbits by 32.00%, 20.46%.

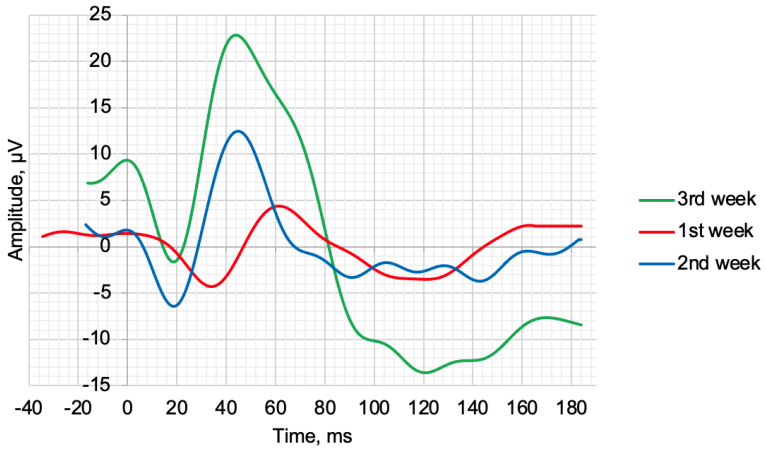

(a)

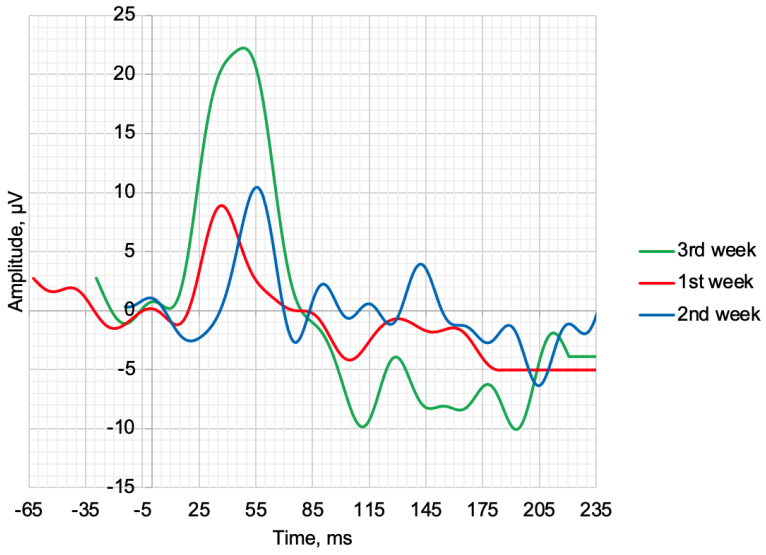

(b)

Figure 2. ERG waveforms in the time-domain representation of rabbit with a weekly interval: (**a**) Scotopic 2.0 ERG Response (**b**) Maximum 2.0 ERG Response

Table 3. Scotopic 2.0 ERG Response and Maximum 2.0 ERG Response parameters of rabbit with a weekly interval.

	1st week	2nd week	3rd week
Maximum 2.0 ERG Response			
a, µV	5.61	8.03	10.81
b, µV	16.48	18.6	24.14
la, ms	33	17.5	20
lb, ms	47	46.5	43
Scotopic 2.0 ERG Response			
a, µV	1.81	3.43	0.75
b, µV	10.26	12.72	21.92
la, ms	13	22.5	8.5
lb, ms	39.5	57.5	50.5

3. Results

3.1. Wavelet scalograms of human and rabbit ERGs signals

Figure 3-Figure 4 show the wavelet scalograms of Maximum 2.0 ERG Response and Scotopic 2.0 ERG Response. The CWT scalograms depict a time-frequency representation, where the horizontal axis denotes time values in milliseconds (ms) and the vertical axis represents frequency values in Hertz (Hz). The Gaussian 8 degree Wavelet figure also displays segment numbering for the corresponding scalogram. To describe the CWT wavelet scalograms uniformly, the scalogram areas into even and odd segments by analogy with the previous study [54]. The spatial arrangement and energy of central segments No. 1-4 were evaluated since segments No. 1-4 have the most physiological information and have a low level of noise associated with eye movement artifacts. In turn, the DWT wavelet scalograms represent the energy (µV·s) within the signal which was extracted for statistical analysis. DWT scalogram presents the energies within each frequency band centered on 20, 40, 80, and 160 Hz. The horizontal axis of the DWT scalogram denotes time values in samples and the vertical axis represents frequency values in Hertz (Hz). It should be noted that the signal was upsampled from 1000 to 1280 Hz to get 20-160 Hz frequency bands.

CWT (Ricker Wavelet) wavelet scalogram in Figure 3 demonstrates significant energy and localization differences between the rabbit and human signals. The area with maximum energy in Adult 1 is in the range of 0-45 ms and 3-67 Hz (segment No.1), 50-100 ms and 3-67 Hz (segment No.2); Child 1 - 18-45 ms and 5-65 Hz (segment No.1), 56-87 ms and 5-65 Hz (segment No.2); Rabbit 1 - 55-65 ms and 8-20 Hz (segment No.2).

CWT (Morlet Wavelet): Adult 1 - 0-45 ms and 5-50 Hz (segment No.1), 50-100 ms and 5-50 Hz (segment No.2); Child 1 - 18-45 ms and 7-50 Hz (segment No.1), 56-80 ms and 7-50 Hz (segment No.2); Rabbit 1 - 60-70 ms and 7-20 Hz (segment No.2).

CWT (Gaussian 8 degree Wavelet): Adult 1 - 0-50 ms and 5-50 Hz (segment No.1), 50-100 ms and 5-50 Hz (segment No.2); Child 1 - 18-45 ms and 5-50 Hz (segment No.1), 55-90 ms and 5-50 Hz (segment No.2); Rabbit 1 - 12-37 ms and 7.8-15 Hz (segment No.1), 55-68 ms and 5-23 Hz (segment No.2).

DWT (Daubechies Wavelet) wavelet scalogram in Figure 3 demonstrates most of the power in the low freq regions: Adult 1 - 0-100 samples for 10 Hz (maximum power), 50-100 samples for 20 Hz (medium power), from 40 Hz (low power); Child 1 - 0-100 samples for 10 Hz (maximum power), 50-100 samples for 20 Hz and 100-200 samples for 10 Hz (medium power), from 40 Hz (low power); Rabbit 1 - 100-200 samples for 10 Hz (maximum power), from 40 Hz (low power).

DWT (Biorthogonal 3.1 Wavelet): Adult 1 - 0-100 samples for 10 Hz (maximum power), 0-50 samples for 20 Hz (medium power), from 40 Hz (low power); Child 1 - 0-100 samples for 10 Hz (maximum power), 0-50 samples for 20 Hz (medium power), from 40 Hz (low power); Rabbit 1 - 0-100 samples for 10 Hz (maximum power), from 20 Hz (low power).

DWT (Haar Wavelet): Adult 1 - 0-100 samples for 10 Hz (maximum power), 0-50 samples for 20 Hz and 50-100 samples for 40 Hz (medium power), from 40 Hz (low power); Child 1 - 0-100 samples for 10 Hz and 0-50 samples for 20 Hz (maximum power), 50-100 samples for 20 Hz and about 70 samples for 40 Hz (medium power), from 80 Hz (low power); Rabbit 1 - 0-100 samples for 10 Hz (maximum power), 100-200 samples for 10 Hz (medium power), from 20 Hz (low power).

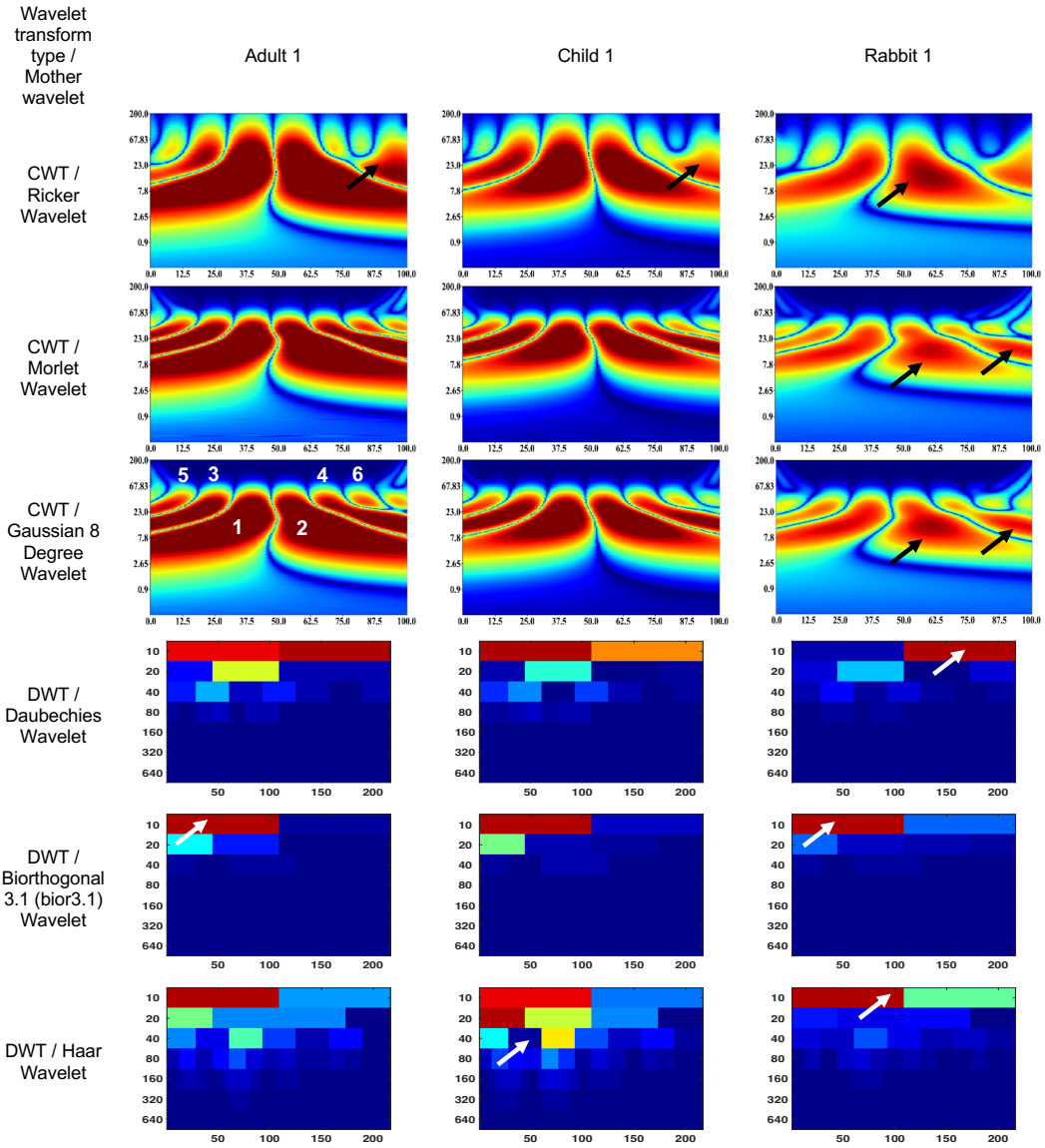

Figure 3. Wavelet scalograms of Maximum 2.0 ERG Response in healthy human and rabbit subjects.

CWT (Ricker Wavelet) wavelet scalogram in Figure 4 shows noticeable variations in energy and location between the signals produced by rabbits and humans. The area with maximum energy in Adult 1 is in the range of 0-130 ms and 1-37 Hz (segment No.1), 150-250 ms and 1-37 Hz (segment No.2); Child 1 - 0-130 ms and 1-37 Hz (segment No.1), 50-250 ms and 1-10 Hz (segment No.2); Rabbit 1 - 20-70 ms and 100-200 Hz (segment No.1), 2-20 ms and 3-16 Hz (segment No.2).

CWT (Morlet Wavelet): Adult 1 - 0-130 ms and 2-16 Hz (segment No.1), 130-250 ms and 2-16 Hz (segment No.2); Child 1 - 0-140 ms and 2-16 Hz (segment No.1), 140-250 ms and 2-14 Hz (segment No.2); Rabbit 1 - 25-75 ms and 3-16 Hz (segment No.1), 100-150 ms and 3-16 Hz (segment No.2).

CWT (Gaussian 8 degree Wavelet): Adult 1 - 0-50 ms and 5-50 Hz (segment No.1), 50-100 ms and 5-50 Hz (segment No.2); Child 1 - 18-45 ms and 5-50 Hz (segment No.1), 55-90 ms and 5-50 Hz (segment No.2); Rabbit 1 - 12-37 ms and 7.8-15 Hz (segment No.1), 55-68 ms and 5-23 Hz (segment No.2).

DWT (Daubechies Wavelet) wavelet scalogram in Figure 4 shows the majority of the energy is concentrated in the lower frequency regions: Adult 1 - 100-300 samples for 10 Hz (maximum power), 450-600 samples for 10 Hz (medium power), from 20 Hz (low power); Child 1 - 100-200 samples for 10 Hz (maximum power), 200-600 samples for 10 Hz (medium power), from 20 Hz (low power); Rabbit 1 - 0-50 samples for 10 Hz (maximum power), 200-300 samples for 10 Hz (medium power), from 20 Hz (low power).

DWT (Biorthogonal 3.1 Wavelet): Adult 1 - 0-200 samples for 10 Hz (maximum power), 300-600 samples for 10 Hz (medium power), from 20 Hz (low power); Child 1 - 0-50 samples for 10 Hz (maximum power), 100-600 samples for 10 Hz (medium power), from 20 Hz (low power); Rabbit 1 - 100-200 samples for 10 Hz (maximum power), 200-300 samples for 10 Hz (medium power), from 20 Hz (low power).

DWT (Haar Wavelet): Adult 1 - 0-100 samples for 10 Hz (maximum power), 400-600 samples for 100 Hz (medium power), from 20 Hz (low power); Child 1 - 0-100 samples for 10 Hz and 300-600 samples for 10 Hz (medium power), from 20 Hz (low power); Rabbit 1 - 0-150 samples for 10 Hz and 100-150 samples for 20 Hz (maximum power), 150-400 samples for 10 Hz (medium power), from 30 Hz (low power).

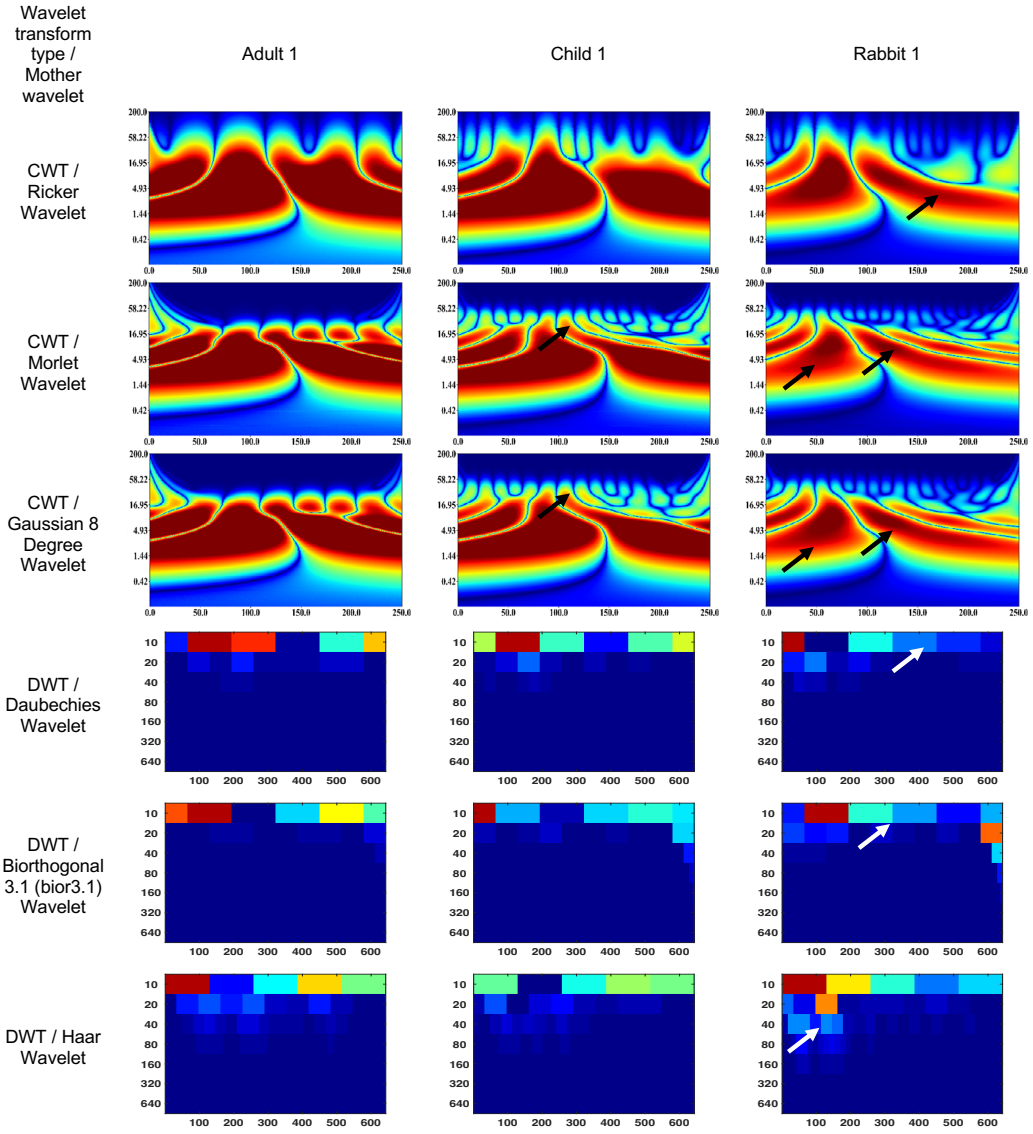

Figure 4. Wavelet scalograms Scotopic 2.0 ERG Response waveforms in healthy human and rabbit subjects.

3.2. Endophthalmitis treatment in rabbit

CWT (Ricker Wavelet) wavelet scalogram in Figure 5 shows treatment for 3 weeks. The area with maximum energy in 1st week is in the range of 0-130 ms and 2-37 Hz (segment No.1), 170-250 ms and 1-5 Hz (segment No.2); 2nd week - 55-70 ms and 5-50 Hz (segment No.1); 3rd week - 0-120 ms and 2-17 Hz (segment No.1), 130-250 ms and 2-15 Hz (segment No.2).

CWT (Morlet Wavelet): 1st week - 80-120 ms and 7-18 Hz (segment No.1), 130-170 ms and 7-18 Hz (segment No.2); 2nd week - 25-80 ms and 2-55 Hz (segment No.1), 80-175 ms and 2-55 Hz (segment No.2); 3rd week - 0-80 ms and 2-18 Hz (segment No.1), 110-200 ms and 2-18 Hz (segment No.2).

CWT (Gaussian 8 degree Wavelet): 1st week - 55-70 ms and 5-11 Hz (segment No.1), 140-160 ms and 6-11 Hz (segment No.2); 2nd week - 60-65 ms and 9-14 Hz (segment No.1), 97-102 ms and 9-14 Hz (segment No. 2); 3rd week - 0-87 ms and 2-18 Hz (segment No.1), 112-200 ms and 2-18 Hz (segment No.2).

DWT (Daubechies Wavelet) wavelet scalogram in Figure 5 indicates that most of the energy is focused in the frequency range that is lower: 1st week - 100-200 samples, 400 samples for 10 Hz (maximum power), 50-200 samples for 20 Hz (medium power), from 40

Hz (low power); 2nd week - 0-100 samples for 10 Hz (maximum power), from 20 Hz (low power); 3rd week - 0-100 samples for 10 Hz (maximum power), 100-400 samples for 10 Hz (medium power), from 20 Hz (low power).

DWT (Biorthogonal 3.1 Wavelet): 1st week - 0-2100 samples for 10 Hz (maximum power), 250-350 samples for 10 Hz (medium power), from 20 Hz (low power); 2nd week - 100-200 samples, 400 samples for 10 Hz and 0-50 samples for 20 Hz (maximum power), 250-350 samples for 10 Hz (medium power), from 40 Hz (low power); 3rd week - 0-100 samples for 10 Hz (maximum power), 100-400 samples for 10 Hz (medium power), from 20 Hz (low power).

DWT (Haar Wavelet): 1st week - 0-100 samples, 250-350 samples for 10 Hz (maximum power), from 20 Hz (low power); 2nd week - 100-350 samples for 10 Hz (medium power), from 80 Hz (low power); 3rd week - 0-100 samples for 10 Hz (maximum power), 250-400 samples for 10 Hz (medium power), from 20 Hz (low power).

It should be noted that the ERG of the 1st week showed a signal shift to the right. The ERG region with maximum energy of the 3rd week corresponds to the frequency characteristics of the rabbit ERG in Figure 3, however, it has a time extension of 50% (segment No.1) and 30% (segment No.2). In addition, the high-frequency component of the signal is more pronounced compared to Figure 3.

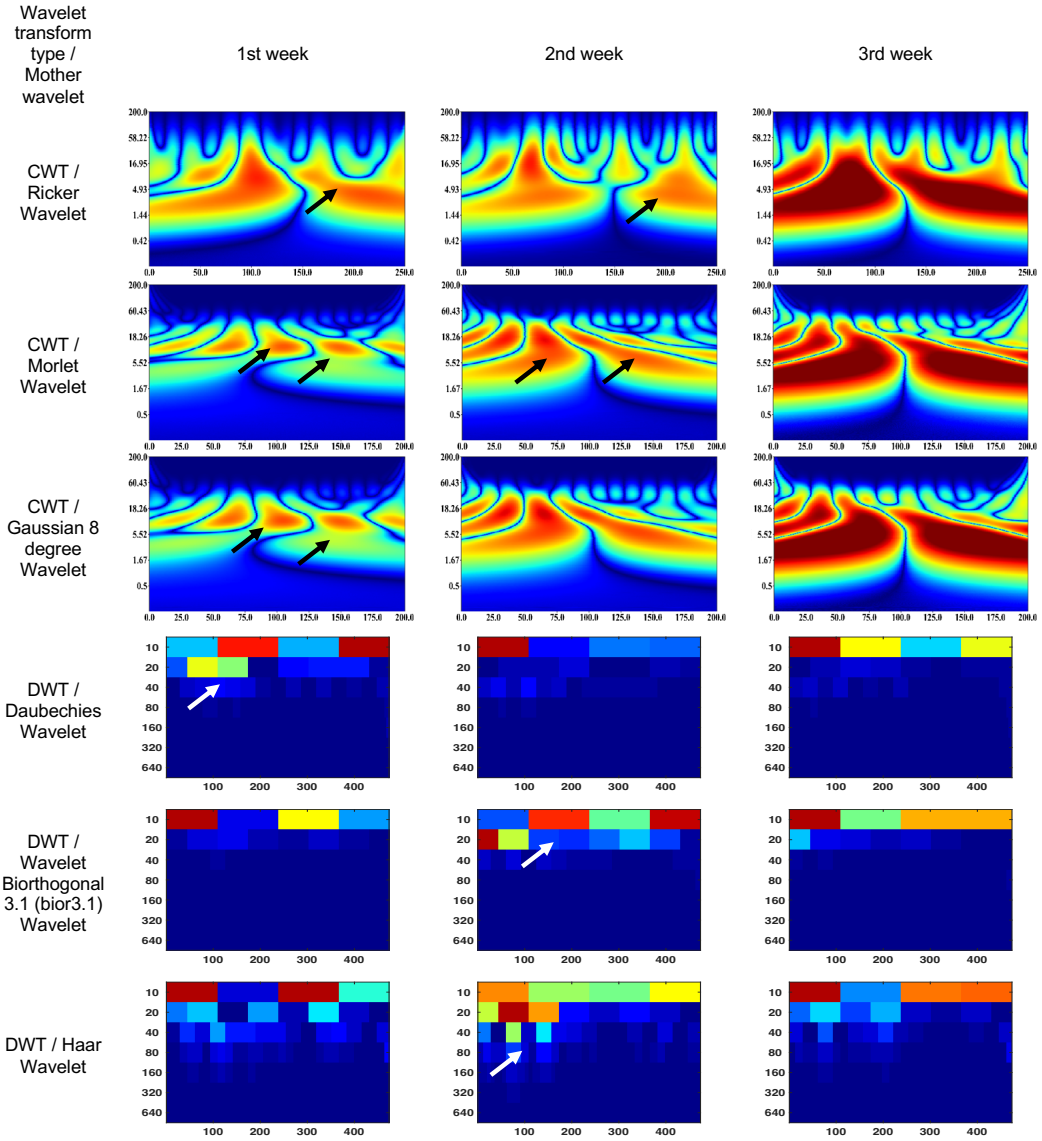

Figure 5. Wavelet scalograms of Maximum 2.0 ERG Response in rabbit following treatment at week 1, 2 and 3.

CWT (Ricker Wavelet) wavelet scalogram in Figure 6 shows treatment for 3 weeks. The area with maximum energy in 1st week is in the range of 25-130 ms and 2-37 Hz (segment No.1), 150-250 ms and 2-16 Hz (segment No.2); 2nd week - 25-130 ms and 2-37 Hz (segment No.1); 3rd week - 0-130 ms and 2-30 Hz (segment No.1), 130-250 ms and 2-16 Hz (segment No.2).

CWT (Morlet Wavelet): 1st week - 75-130 ms and 5-16 Hz (segment No.1), 150-175 ms and 5-16 Hz (segment No.2); 2nd week - scalogram segments are not differentiable and represent sets of spots or discontinuities in the signal, corresponding to different scales and frequencies; 3rd week - 0-130 ms and 2-16 Hz (segment No.1), 130-250 ms and 2-16 Hz (segment No.2).

CWT (Gaussian 8 degree Wavelet): 1st week - 4-10 ms and 90-110 Hz (segment No.1); 2nd week - scalogram segments are not differentiable and represent sets of spots or discontinuities in the signal, corresponding to different scales and frequencies; 3rd week - 1-17 ms and 0-110 Hz (segment No.1), 1-17 ms and 0-110 Hz (segment No.2)

DWT (Daubechies Wavelet) wavelet scalogram in Figure 6 indicates that the majority of the energy is concentrated in the lower frequency range: 1st week - 0-50 samples for 10 Hz (maximum power), 50-100 samples for 20 Hz (medium power), from 40 Hz (low

power); 2nd week - 0-50 samples for 10 Hz and 100-150 samples for 20 Hz (maximum power), 100-200 samples for 10 Hz (medium power), from 20 Hz (low power); 3rd week - 0-50 samples for 10 Hz (maximum power), 50-200 samples for 10 Hz (medium power), from 20 Hz (low power).

DWT (Biorthogonal 3.1 Wavelet): 1st week - 550-600 samples for 10 Hz (maximum power), 200-300 samples for 10 Hz (medium power), from 20 Hz (low power); 2nd week - 0-50 samples for 10 Hz (maximum power), 100-150 samples for 20 Hz (medium power), from 40 Hz (low power); 3rd week - 0-50 samples for 10 Hz (maximum power), 200-600 samples for 10 Hz (medium power), from 20 Hz (low power).

DWT (Haar Wavelet): 1st week - 550-600 samples for 10 Hz (maximum power), 200-550 samples for 10 Hz (medium power), from 20 Hz (low power); 2nd week - 0-50 samples for 10 Hz (maximum power), 100-200 samples for 20 Hz (medium power), from 40 Hz (low power); 3rd week - 0-50 samples for 10 Hz and 150-200 samples for 20 Hz (maximum power), 200-600 samples for 10 Hz (medium power), from 40 Hz (low power).

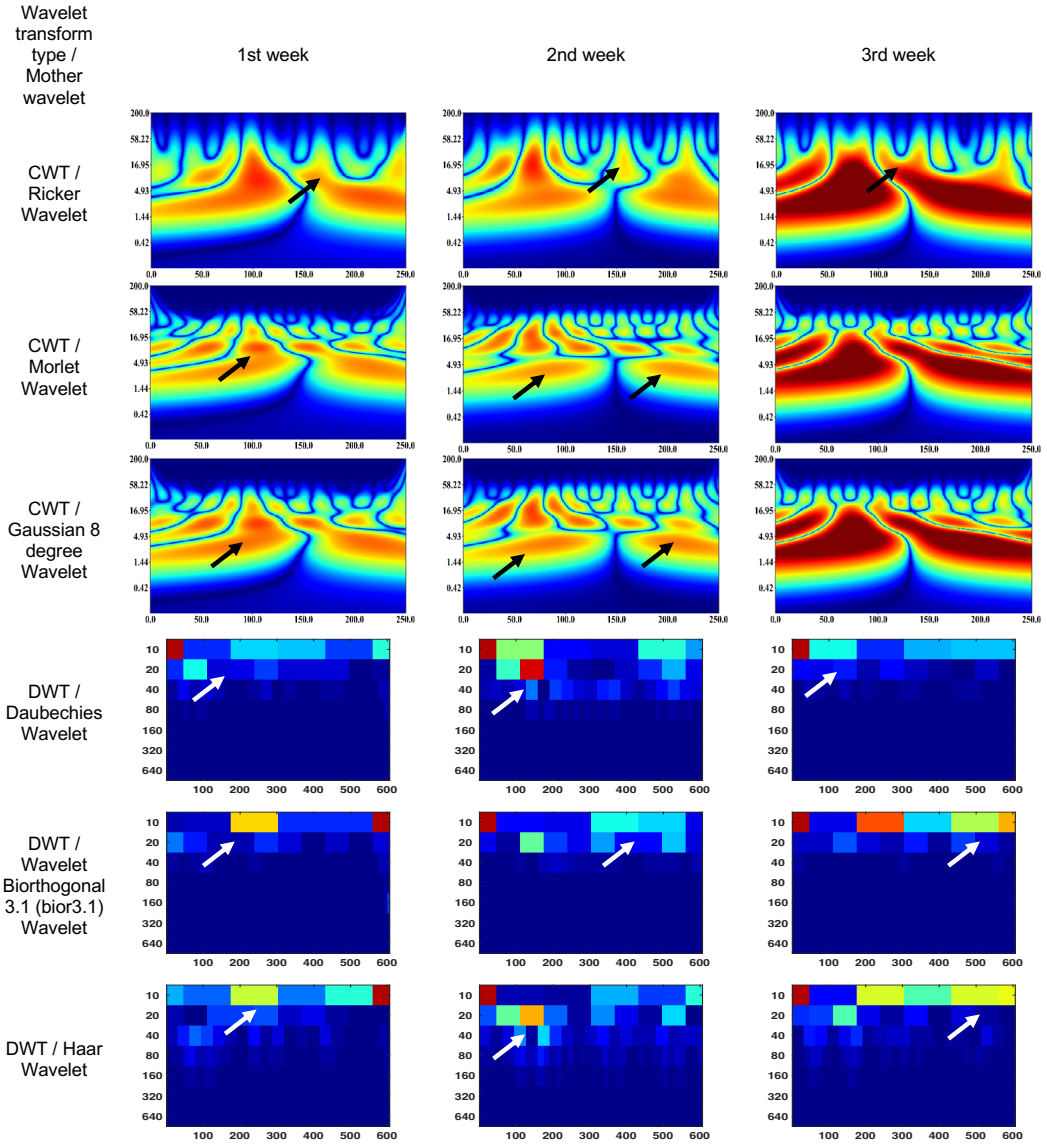

Figure 6. Wavelet scalograms of Scotopic 2.0 ERG Response in rabbit following treatment at week 1, 2 and 3..

4. Discussion

The mother wavelets used in the study are similar in form and parameters to the ERG, in particular, their impulsive nature. For example, the difference between the Morlet wavelet and the Gaussian wavelet is that the Morlet wavelet has better selectivity properties in the frequency domain, while the Gaussian wavelet has better properties in the time domain. However, it is proving elusive to obtain localization of an ideal character simultaneously in the frequency and time domains.

The basis functions of CWT, in most cases, are not strictly orthogonally normalized due to the fact that the elements of the basis are infinitely differentiated with exponential characteristics falling off at time infinity. DWT does not have the above problems due to the higher accuracy of the reconstruction of the studied signals. The choice of the type and typology of wavelets primarily depends on the studied ERG signal and the task of this analysis taking into account the level of knowledge and experience of the researcher.

Therefore, it is necessary to pay attention to verification and determining the level of the biomedical signal's effectiveness. It should be noted that when using a similar ERG analysis of other protocols, different results may be obtained in practical terms.

5. Conclusions

5.1. Human and rabbit ERG signals

In the given context, the comparison of Adult, Child, and Rabbit ERG responses in CWT showed that the power of Adult signals in segments No.1 and 2 was significantly higher than that of Child signals which aligns with the larger ERG amplitudes observed in the adult subjects. Additionally, Rabbit signals exhibited a less pronounced a-wave in segment No.1 and a less pronounced b-wave in segment No.2, with the magnitude of the effect being dependent on the state of retinal adaption and amplitude of the response. The differences in the spectral composition of the ERGs between rabbit and human are of note and may be the result of differences in retinal morphology and may have implications for studies involving rabbit models of retinal pathology [57,58]. The Morlet Wavelet and Gaussian 8 degree Wavelet are commonly used in signal processing applications and have been found to have similar performance in extracting parameters from the scalogram, providing a visual representation of a signal's time-frequency components. However, in the analysis of electrophysiological signals such as Adult, Child, and Rabbit signals, it has been observed that DWT tends to exhibit low-frequency components due to the presence of software filtering in the electrophysiology equipment used. In contrast, the Haar Wavelet has been found to provide superior visualization of frequency components in such signals.

Experimental studies in ophthalmology are often performed on the eyes of rabbits due to the convenience of work (the size of the eyeball is similar to the human eye and the possibility of clinical observation without additional specialized equipment) [51]. On the other hand, the rabbit retina has significant differences from the human retina (merangiotic type of the retina, absence of the macular area, different distribution of photoreceptors of various types) [52,53]. Nevertheless, the results obtained in the study demonstrate the possibility of quantifying functional changes in the time domain and time-frequency domain representation in the rabbit ERG under scotopic and photopic conditions. However, caution should be taken as the features observed using signal analysis show differences to the human ERGs despite a similar shape under photopic and scotopic conditions.

5.2. Endophthalmitis treatment in rabbit

The results obtained from CWT indicate that the pathological states exhibit a marked differentiation of segments, leading to the formation of low-power patches. On the other hand, DWT analysis demonstrated a non-linear and irregular distribution of signal frequency components under pathological conditions.

Figure 7 shows the data OCT and SLP images of rabbit at weekly intervals. There are positive changes in the structures of the anterior segment of the eye during treatment according to SLP. The preservation of the normal anatomy of the sensory retina of the

posterior segment of the eye is observed. Hyper-reflective dots in the preretinal region were only registered in 1st week according to OCT.

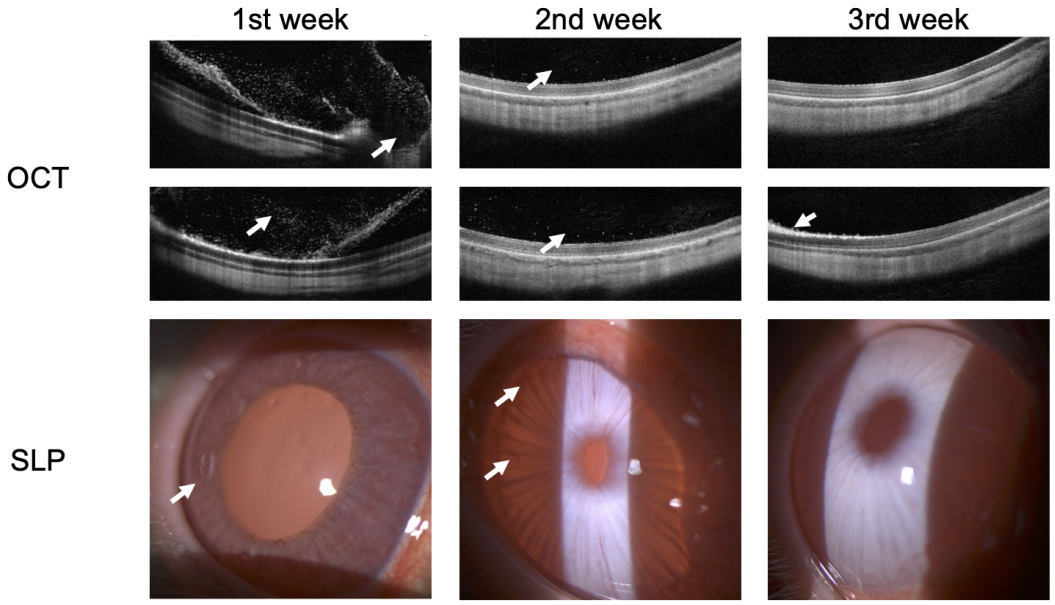

Figure 7. OCT and SLP images of rabbit at weekly intervals. Arrows indicate main anatomical changes following treatment.

1st week: Massive hyperreflective elements and preretinal macular membrane formation were visualized in the posterior segment of the eye using OCT scans. In turn, pericorneal injection, and increased iris pastosity along with newly formed vessels of the iris were visualized in the anterior segment of the eye using SLP.

2nd week: Decreased hyperreflective elements allowed for assessing the photoreceptor's destruction articulation and the pigment epithelium complex - Bruch's membrane was now visible with decreased iris pastosity along with the number of new vessels in the anterior segment of the eye.

3rd week: Normalizing of the posterior segment of the eye was visualized except for a single foci of photoreceptor damage. The condition of the anterior segment of the eye corresponded to the control eye according to SLP data.

Thus, the results SLP and OCT confirm that ERG rabbit did not show a pronounced decrease in the main indicators of the electrobiological activity of the retina.

Author Contributions: Conceptualization, A.Z.; methodology, A.Z. and P.C.; software, S.MM. and A.D.; validation, A.Z., P.C.; formal analysis, A.Z. and P.C.; investigation, A.Z., P.C., S.MM. and A.D.; resources, A.Z., P.C.; data curation, P.C., H.PQ.; writing—original draft preparation, A.Z., P.C. and A.L.; writing—review and editing, A.Z., P.C.; visualization, S.MM., A.D. and A.Z.; supervision, A.Z.; project administration, A.Z.; funding acquisition, A.Z. All authors have read and agreed to the published version of the manuscript.

Funding: The research funding from the Ministry of Science and Higher Education of the Russian Federation (Ural Federal University Program of Development within the Priority—2030 Program) is gratefully acknowledged.

Institutional Review Board Statement: The study was approved by the ethics committee of Ural Federal University Named after the First President of Russia B. N. Yeltsin (Conclusion No. 1 dated 1 February 2021).

Informed Consent Statement: Informed consent was obtained from all subjects involved in the study.

Data Availability Statement: Zhdanov, A.E.; Dolganov, A.Y.; Borisov, V.I.; Lucian, E.; Bao, X.; Kazaijkin, V.N.; Ponomarev, V.O.; Lizunov, A.V.; Ivliev, S.A. OculusGraphy: Pediatric and Adults Electroretinograms Database, 2020. https://doi.org/10.21227/y0fh-5v04 (accessed on 29 November 2022).

Acknowledgments: Aleksei Zhdanov executed the design, the definition of intellectual content, data analysis, and manuscript preparation and editing within the Bi-nationally Supervised Doctoral Degrees/Cotutelle DAAD Research Grant.

Conflicts of Interest: The authors declare that they have no known competing financial interest or personal relationships that could have appeared to influence the work reported in this paper.

Abbreviations

The following abbreviations are used in this manuscript:

LA	Light Adapted
OPs	Oscillatory Potentials
DWT	Discrete Wavelet Transform
CWT	Continuous Wavelet Transform
SLP	Slit-lamp Photography
OCT	Optical Coherence Tomography

References

1. Robson, A.G., Frishman, L.J., Grigg, J., Hamilton, R., Jeffrey, B.G., Kondo, M., et al. (2022). ISCEV Standard for full-field clinical electroretinography (2022 update). *Doc Ophthalmol* **144**(3), 165-177. doi: 10.1007/s10633-022-09872-0.
2. Robson, A.G., Nilsson, J., Li, S., Jalali, S., Fulton, A.B., Tormene, A.P., et al. (2018). ISCEV guide to visual electrodiagnostic procedures. *Doc Ophthalmol* **136**(1), 1-26. doi: 10.1007/s10633-017-9621-y.
3. Granit, R. (1950). Physiology of Vision. *Annu Rev Physiol* **12**, 485-502. doi: 10.1146/annurev.ph.12.030150.002413.
4. Baylor, D.A., Lamb, T.D., and Yau, K.W. (1979). The membrane current of single rod outer segments. *J Physiol* **288**, 589-611.
5. Robson, J.G., Saszik, S.M., Ahmed, J., and Frishman, L.J. (2003). Rod and cone contributions to the a-wave of the electroretinogram of the macaque. *J Physiol* **547**(Pt 2), 509-530. doi: 10.1113/jphysiol.2002.030304.
6. Robson, J.G., and Frishman, L.J. (2014). The rod-driven a-wave of the dark-adapted mammalian electroretinogram. *Prog Retin Eye Res* **39**, 1-22. doi: 10.1016/j.preteyeres.2013.12.003.
7. Knapp, A.G., and Schiller, P.H. (1984). The contribution of on-bipolar cells to the electroretinogram of rabbits and monkeys. A study using 2-amino-4-phosphonobutyrate (APB). *Vision Res* **24**(12), 1841-1846. doi: 10.1016/0042-6989(84)90016-6.
8. Heynen, H.; van Norren, D. Origin of the electroretinogram in the intact macaque eye–II. Current source-density analysis. *Vision Res* **1985**, *25* (5), 709–715. doi:10.1016/0042-6989(85)90177-4.
9. Thompson, D.A.; Feather, S.; Stanescu, H.C.; Freudenthal, B.; Zdebik, A.A.; Warth, R.; et al. Altered electroretinograms in patients with KCNJ10 mutations and EAST syndrome. *J Physiol* **2011**, *589* (Pt 7), 1681–1689. doi:10.1113/jphysiol.2010.198531.
10. Diamond, J.S. Inhibitory Interneurons in the Retina: Types, Circuitry, and Function. *Annu Rev Vis Sci* **2017**, *3*, 1–24. doi:10.1146/annurev-vision-102016-061345.
11. Barnes, S.; Grove, J.C.R.; McHugh, C.F.; Hirano, A.A.; Brecha, N.C. Horizontal Cell Feedback to Cone Photoreceptors in Mammalian Retina: Novel Insights From the GABA-pH Hybrid Model. *Front Cell Neurosci* **2020**, *14*, 595064. doi:10.3389/fncel.2020.595064.
12. Bush, R.A.; Sieving, P.A. A proximal retinal component in the primate photopic ERG a-wave. *Investigative Ophthalmology Visual Science* **1994**, *35* (2), 635–645.
13. Gouras, P.; MacKay, C. A new component in the a-wave of the human cone electroretinogram. *Doc Ophthalmol* **2000**, *101* (1), 19–24.
14. Dang, T.M.; Tsai, T.I.; Vingrys, A.J.; Bui, B.V. Post-receptoral contributions to the rat scotopic electroretinogram a-wave. *Doc Ophthalmol* **2011**, *122* (3), 149–156. doi:10.1007/s10633-011-9269-y.
15. Diamond, J.S. Inhibitory Interneurons in the Retina: Types, Circuitry, and Function. *Annu Rev Vis Sci* **2017**, *3*, 1–24. doi: 10.1146/annurev-vision-102016-061345.
16. Hirano, A.A.; Vuong, H.E.; Kornmann, H.L.; Schietroma, C.; Stella, S.L., Jr.; Barnes, S.; Brecha, N.C. Vesicular Release of GABA by Mammalian Horizontal Cells Mediates Inhibitory Output to Photoreceptors. *Front Cell Neurosci* **2020**, *14*, 600777. doi: 10.3389/fncel.2020.600777.
17. Viswanathan, S.; Frishman, L.J.; Robson, J.G.; Walters, J.W. The photopic negative response of the flash electroretinogram in primary open angle glaucoma. *Invest Ophthalmol Vis Sci* **2001**, *42*, 514–522.
18. Wachtmeister, L.; Dowling, J.E. The oscillatory potentials of the mudpuppy retina. *Invest Ophthalmol Vis Sci* **1978**, *17*, 1176–1188.
19. Wachtmeister, L. Further studies of the chemical sensitivity of the oscillatory potentials of the electroretinogram (ERG) I. GABA- and glycine antagonists. *Acta Ophthalmol (Copenh)* **1980**, *58*, 712–725. doi: 10.1111/j.1755-3768.1980.tb06684.x.

20. Wachtmeister, L. Further studies of the chemical sensitivity of the oscillatory potentials of the electroretinogram (ERG). II. Glutamate-aspartate-and dopamine antagonists. *Acta Ophthalmol (Copenh)* **1981**, *59*, 247–258. doi: 10.1111/j.1755-3768.1981.tb02987.x.
21. Wachtmeister, L. Oscillatory potentials in the retina: what do they reveal. *Prog Retin Eye Res* **1998**, *17*, 485–521. doi: 10.1016/s1350-9462(98)00006-8.
22. Diamond, J.S. Inhibitory Interneurons in the Retina: Types, Circuitry, and Function. *Annu Rev Vis Sci* **2017**, *3*, 1-24. https://doi.org/10.1146/annurev-vision-102016-061345.
23. Knapp, A.G.; Schiller, P.H. The contribution of on-bipolar cells to the electroretinogram of rabbits and monkeys. A study using 2-amino-4-phosphonobutyrate (APB). *Vision Res* **1984**, *24*(12), 1841-1846. https://doi.org/10.1016/0042-6989(84)90016-6.
24. Dong, C.J.; Agey, P.; Hare, W.A. Origins of the electroretinogram oscillatory potentials in the rabbit retina. *Vis Neurosci* **2004**, *21*(4), 533-543.
25. Yin, L.; Pi, Y.L.; Zhang, M.N. The effect of Vaccinium uliginosum on rabbit retinal structure and light-induced function damage. *Chin J Integr Med* **2012**, *18*(4), 299-303. https://doi.org/10.1007/s11655-011-0901-1.
26. Myers, A.C.; Bruun, A.; Ghosh, F.; Adrian, M. L.; Andreasson, S.; Ponjavic, V. Intravitreal injection of triamcinolone acetonide into healthy rabbit eyes alters retinal function and morphology. *Curr Eye Res* **2013**, *38*(6), 649-661. https://doi.org/10.3109/02713683.2012.750367.
27. Pochop, P.; Darsova, D.; Uhlik, J.; Lestak, J.; Kukaka, J.; Kodetova, D.; et al. Retinal toxicity after repeated intravitreal carboplatin injection into rabbit eyes. *Biomed Pap Med Fac Univ Palacky Olomouc Czech Repub* **2014**, *158*(4), 552-556. https://doi.org/10.5507/bp.2012.106.
28. Smith, N.P.; Lamb, T.D. The a-wave of the human electroretinogram recorded with a minimally invasive technique. *Vision Res* **1997**, *37*(21), 2943-2952. https://doi.org/10.1016/S0042-6989(97)00124-6.
29. Friedburg, C., Allen, C.P., Mason, P.J., and Lamb, T.D. Contribution of cone photoreceptors and post-receptor mechanisms to the human photopic electroretinogram. *J Physiol* **2004**, *556*(Pt 3), 819-834. https://doi.org/10.1113/jphysiol.2004.061523.
30. Mahroo, O.A.; Ban, V.S.; Bussmann, B.M.; Copley, H.C.; Hammond, C.J.; Lamb, T.D. Modeling the initial phase of the human rod photoreceptor response to the onset of steady illumination. *Doc Ophthalmol* **2012**, *124*(2), 125-131. https://doi.org/10.1007/s10633-012-9316-3.
31. Forte, J.D.; Bui, B.V.; Vingrys, A.J. Wavelet analysis reveals dynamics of rat oscillatory potentials. *J Neurosci Methods* **2008**, *169*(1), 191-200. https://doi.org/10.1016/j.jneumeth.2007.12.007.
32. Gauvin, M.; Dorfman, A.L.; Trang, N.; Gauthier, M.; Little, J.M.; Lina, J.M.; et al. Assessing the Contribution of the Oscillatory Potentials to the Genesis of the Photopic ERG with the Discrete Wavelet Transform. *Biomed Res Int* **2016**, *2016*, 2790194. https://doi.org/10.1155/2016/2790194.
33. Rufiange, M.; Dassa, J.; Dembinska, O.; Koenekoop, R.K.; Little, J.M.; Polomeno, R.C.; et al. The photopic ERG luminance-response function (photopic hill): method of analysis and clinical application. *Vision Res* **2003**, *43*(12), 1405-1412. https://doi.org/10.1016/S0042-6989(03)00206-2.
34. Hamilton, R.; Bees, M.A.; Chaplin, C.A.; McCulloch, D.L. The luminance-response function of the human photopic electroretinogram: a mathematical model. *Vision Res* **2007**, *47*(23), 2968-2972. doi: 10.1016/j.visres.2007.04.020.
35. Johnson, M.A.; Jeffrey, B.G.; Messias, A.M.V.; Robson, A.G. ISCEV extended protocol for the stimulus–response series for the dark-adapted full-field ERG b-wave. *Doc Ophthalmol* **2019**, *138*(3), 217-227. doi: 10.1007/s10633-019-09687-6.
36. Garon, M.L.; Dorfman, A.L.; Racine, J.; Koenekoop, R.K.; Little, J.M.; Lachapelle, P. Estimating ON and OFF contributions to the photopic hill: normative data and clinical applications. *Doc Ophthalmol* **2014**, *129*(1), 9-16. doi: 10.1007/s10633-014-9446-x.
37. Constable, P.A.; Gaigg, S.B.; Bowler, D.M.; Jagle, H.; Thompson, D.A. Full-field electroretinogram in autism spectrum disorder. *Doc Ophthalmol* **2016**, *132*(2), 83-99. doi: 10.1007/s10633-016-9529-y.
38. Constable, P.A.; Marmolejo-Ramos, F.; Gauthier, M.; Lee, I.O.; Skuse, D.H.; Thompson, D.A. Discrete Wavelet Transform Analysis of the Electroretinogram in Autism Spectrum Disorder and Attention Deficit Hyperactivity Disorder. *Frontiers in Neuroscience* **2022**, *16*, doi: 10.3389/fnins.2022.890461.
39. Gauvin, M.; Lina, J.M.; Lachapelle, P. Advance in ERG analysis: from peak time and amplitude to frequency, power, and energy. *Biomed Res Int* **2014**, *2014*, 246096. doi: 10.1155/2014/246096.
40. Gauvin, M.; Little, J.M.; Lina, J.M.; Lachapelle, P. Functional decomposition of the human ERG based on the discrete wavelet transform. *J Vis* **2015**, *15*(16), 14. doi: 10.1167/15.16.14.
41. Gauvin, M.; Sustar, M.; Little, J.M.; Brecelj, J.; Lina, J.M.; Lachapelle, P. Quantifying the ON and OFF Contributions to the Flash ERG with the Discrete Wavelet Transform. *Transl. Vis. Sci. Technol.* **2017**, *6*, 3. doi:10.1167/tvst.6.1.3.
42. Brandao, L.M.; Monhart, M.; Schötzau, A.; Ledolter, A.A.; Palmowski-Wolfe, A.M. Wavelet decomposition analysis in the two-flash multifocal ERG in early glaucoma: a comparison to ganglion cell analysis and visual field. *Doc. Ophthalmol.* **2017**, *135*, 29-42. doi:10.1007/s10633-017-9593-y.
43. Dorfman, A.L.; Gauvin, M.; Vatcher, D.; Little, J.M.; Polomeno, R.C.; Lachapelle, P. Ring analysis of multifocal oscillatory potentials (mfOPs) in cCSNB suggests near-normal ON-OFF pathways at the fovea only. *Doc. Ophthalmol.* **2020**, *141*, 99-109. doi:10.1007/s10633-020-09755-2.

44. Mohammad-Manjur, S.; Hossain, M.-B.; Constable, P.A.; Thompson, D.A.; Marmolejo-Ramos, F.; Lee, I.O.; et al. Detecting Autism Spectrum Disorder Using Spectral Analysis of Electroretinogram and Machine Learning: Preliminary results. *IEEE Trans. Biomed. Eng.*
45. Sarossy, M.; Crowston, J.; Kumar, D.; Weymouth, A.; Wu, Z. Time-Frequency Analysis of ERG With Discrete Wavelet Transform and Matching Pursuits for Glaucoma. *Transl. Vis. Sci. Technol.* **2022**, *11*, 19. doi:10.1167/tvst.11.10.19.
46. Hamilton, R. (2021). Clinical electrophysiology of vision-commentary on current status and future prospects. *Eye (Lond)*, *35*(9), 2341-2343. doi: 10.1038/s41433-021-01592-0.
47. Yip, Y. W. Y., Man, T. C., Pang, C. P., Brelen, M. E. (2018). Improving the quality of electroretinogram recordings using active electrodes. *Experimental Eye Research*, *176*, 46-52.
48. Zhdanov, A. E., Dolganov, A. Y., Zanca, D., Borisov, V. I., Lucian, E., Dorosinskiy, L. G. (2023). Evaluation of the effectiveness of the decision support algorithm for physicians in retinal dystrophy using machine learning methods. *Computer Optics*, *47*(2), 272-277.
49. Behbahani, S., Ahmadieh, H., Rajan, S. (2021). Feature Extraction Methods for Electroretinogram Signal Analysis: A Review. *IEEE Access*, *9*, 116879-116897.
50. Ponomarev, V.O., Kazaykin, V.N., Lizunov, A.V., Vokhmintsev, A.S., Vainshtein, I.A., Dezhurov, S.V., Marysheva, V.V. (2021). Evaluation of the Ophthalmotoxic Effect of Quantum Dots InP/ZnSe/ZnS 660 and Bioconjugates Based on Them in Terms of the Prospects for the Treatment of Resistant Endophthalmitis. experimental research. Part 2 (Stage 1). *Ophthalmology in Russia*, *18*(4), 876-884.
51. Ozkan, J., Majzoub, M. E., Coroneo, M., Thomas, T., Willcox, M. (2021). Comparative analysis of ocular surface tissue microbiome in human, mouse, rabbit, and guinea pig. *Experimental Eye Research*, *207*, 108609.
52. Famiglietti, E. V., Sharpe, S. J. (1995). Regional topography of rod and immunocytochemically characterized "blue" and "green" cone photoreceptors in rabbit retina. *Visual neuroscience*, *12*(6), 1151-1175.
53. Williams, D. L. (2012). The rabbit eye. In J. E. Cooper, M. R. L. Thomas (Eds.), *Ophthalmology of Exotic Pets* (pp. 15-55). Wiley-Blackwell.
54. Zhdanov, A., Dolganov, A., Zanca, D., Borisov, V., Ronkin, M. (2022). Advanced Analysis of Electroretinograms Based on Wavelet Scalogram Processing. *Applied Sciences*, *12*(23), 12365.
55. Hamilton, R. (2021). Clinical electrophysiology of vision—commentary on current status and future prospects. *Eye*, *35*(9), 2341-2343.
56. Mahroo, O. A. (2023). Visual electrophysiology and "the potential of the potentials." *Eye*, 1-10.
57. Kondo, M. I. N. E. O. (2010). Animal models of human retinal and optic nerve diseases analyzed using electroretinography. *Nippon Ganka Gakkai Zasshi*, *114*(3), 248-78.
58. Ciulla, T. A., Criswell, M. H., Danis, R. P., Hill, T. E., Introne, W. J. (2000). Endothelin-1-mediated retinal artery vasospasm and the rabbit electroretinogram. *Journal of ocular pharmacology and therapeutics*, *16*(4), 393-398.
59. Ponomarev, V.O., Kazaykin, V.N., Lizunov, A.V., Vokhmintsev, A.S., Vainshtein, I.A., Dezhurov, S.V., Marysheva, V.V. (2021). Evaluation of the Ophthalmotoxic Effect of Quantum Dots InP/ZnSe/ZnS 660 and Bioconjugates Based on Them in Terms of the Prospects for the Treatment of Resistant Endophthalmitis. Experimental Research. Part 2 (Stage 1). *Ophthalmology in Russia*, *18*(4), 876-884.